Journal of Nuclear Materials 414 (2011) 73–82

Contents lists available at ScienceDirect

Journal of Nuclear Materials

journal homepage: www.elsevier.com/locate/jnucmat

Presented at the NuMat 2010 Conference, 4–7 October 2010, Karlsruhe

Controlled oxidation experiments of simulated irradiated UO_2 fuel in relation to thermochemical modelling

E.C. Corcoran [a,*], B.J. Lewis [a], W.T. Thompson [a], J. Mouris [b], Z. He [b]

[a] Department of Chemistry and Chemical Engineering, Royal Military College of Canada, P.O. Box 17000, St. Forces, Kingston, Ont., Canada K7K 7B4
[b] Atomic Energy of Canada Ltd., Chalk River Laboratories, Chalk River, Ont., Canada K0J 1J0

ARTICLE INFO

Article history:
Received 27 September 2010
Accepted 25 November 2010
Available online 4 December 2010

ABSTRACT

A thermochemical model to describe the chemical state of irradiated nuclear fuel has been advanced and validated by comparison to results of experiments on naturally-enriched UO_2 with additions of selected simulated fission products. These experiments involved controlled oxidation in $Ar/H_2O/H_2$ gas mixtures conducted at the Atomic Energy of Canada Limited–Chalk River Laboratories. A coulombic titration technique provided measurements of moles of oxygen acquired by the samples in relation to oxygen potential. Emphasis was placed on the role of molybdenum in buffering the oxidation of fuel.

This treatment is expected to be especially useful when integrated into fuel performance codes that make use of thermodynamics as boundary conditions in heat and mass transfer computations.

Crown Copyright © 2010 Published by Elsevier B.V. All rights reserved.

1. Introduction

The fissioning of oxide fuels generates a multi-component system of more than 40 elements [1,2]. The fission products may be distributed among several phases depending on the temperature, pressure, and composition (burnup) of the fuel-element system. The chemical state of the fuel influences the physical properties including the thermal conductivity, swelling, and melting point, as well as the potential release of fission products for both normal operation and transient conditions [3]. Gaseous fission products (xenon and krypton) released to the fuel-to-clad gap and plenum regions strongly influence the thermal conductance in the fuel-to-clad gap, internal gas pressure and stresses on the cladding. In addition, the knowledge of the chemical state of fission products in irradiated fuels and the conditions that cause them is of importance in interpreting post-irradiation examination data of discharged fuel, long-term spent fuel storage, and possible reprocessing [4,5].

The chemical state of the fuel and fission products is typically determined from out-of-pile release experiments, dissolution experiments, post-irradiation and metallographic examination [6–10]. Theoretical methods have also been used to complement such examinations, where it is implicitly assumed that the system is in thermodynamic equilibrium [11,12]. Progress in the development of a reasonably comprehensive thermodynamic model for irradiated fuel at the Royal Military College of Canada, encompassing the U–O system, and the fission product and actinide components is reviewed in Ref. [11]. This model is built on a large body of existing experimentally determined properties for individual compounds brought together within the framework of classical thermodynamics using Gibbs energy minimization [11]. The model is designed to predict the phases and proportions for twenty-three[1] of the most abundant elements, fission products and activation products.

The thermodynamic data for the thermodynamic model are critically assessed in Ref. [13], and summarized in Ref. [14]. These data are used to generate Gibbs energy functions to compute the proportions and composition of each phase at a given fuel burnup using a Gibbs energy minimizer. In particular, when many elements are involved in possible reactions, and particularly when more than one phase may arise, a Gibbs energy minimizer can be used to systematically redistribute the elements among the many possible compounds in such a way as to preserve the number of moles of each element in a closed system. For each possible distribution, at the chosen temperature and pressure, the Gibbs energy change is computed relative to the previous distribution. This process continues until the Gibbs energy is no longer significantly reduced [15,16].

The model can also be used to predict the oxygen potential for fuel that contains fission products when exposed to a gas of a specified oxygen partial pressure at a known temperature in order to

* Corresponding author.
E-mail address: emily.corcoran@rmc.ca (E.C. Corcoran).

[1] U, Zr, Mo, Ce, Ru, Sr, Ba, La, Nd, Pd, Rh, Cs, Pu, Xe, Np, Y, Tc, Pr, Rb, Te, I, H and O.

0022-3115/$ - see front matter Crown Copyright © 2010 Published by Elsevier B.V. All rights reserved.
doi:10.1016/j.jnucmat.2010.11.063

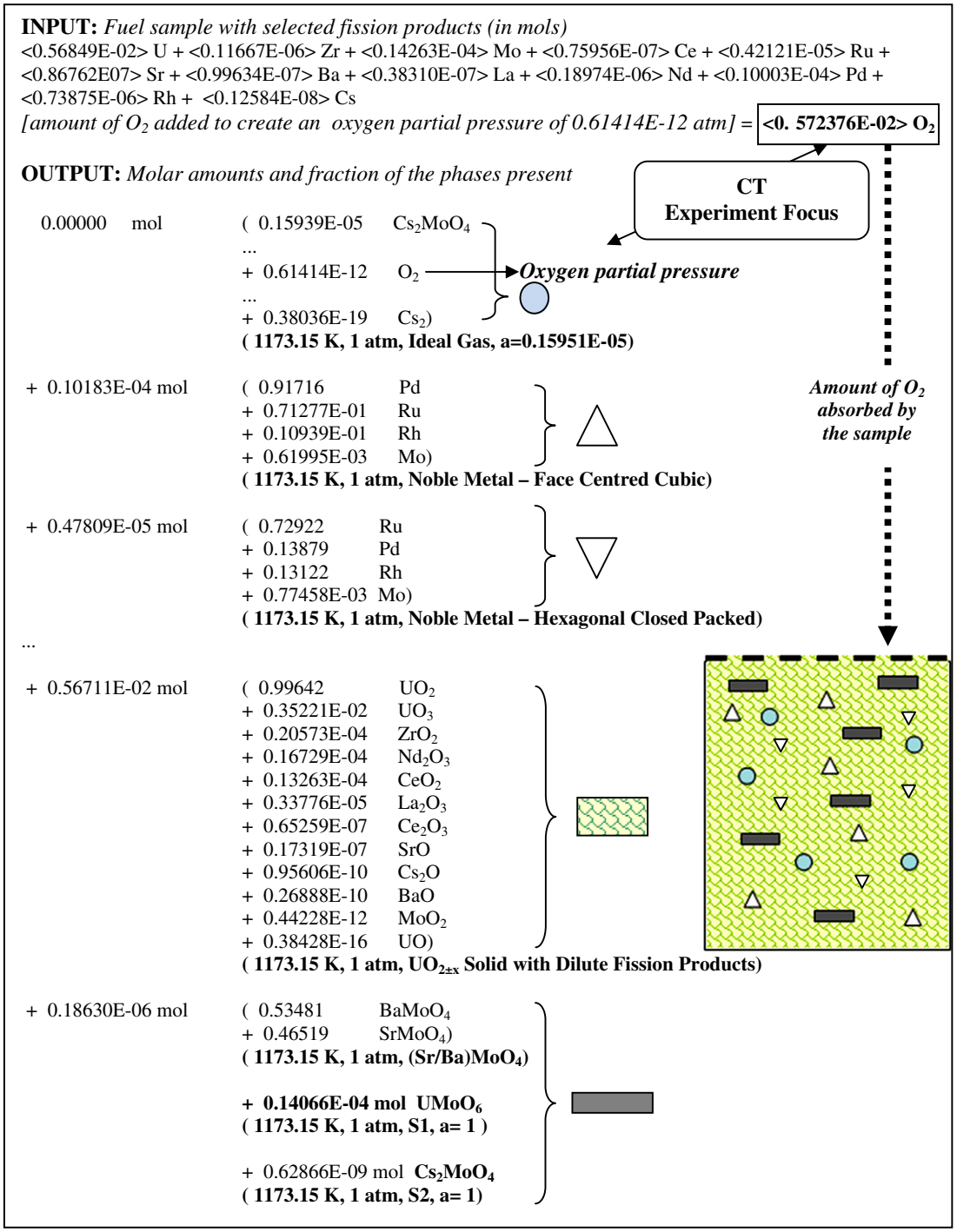

Fig. 1. Predicted phase and phase proportions for four-additive SIMFUEL at 1173 K, 1 atm exposed to an oxygen partial pressure of 0.61414E−12 atm.

assess the effects of fuel oxidation in defective fuel elements [17]. To illustrate the model capabilities, the model is used to simulate fuel samples of simulated burnup containing various fission product additives (i.e., SIMFUEL [18]). In particular, experiments, as detailed in Section 3, are used to specifically benchmark the proposed model. A representative case with four fission product additives for the SIMFUEL sample is listed in Fig. 1, which shows input and output compositions. The calculation shown in Fig. 1 provides the number of moles of oxygen (0.572376×10^{-2} mol) acquired by a 1520.42 mg SIMFUEL sample at an oxygen partial pressure of 0.61414×10^{-12} atm at a temperature of 1173 K. Fig. 1 summarizes the quantity of each phase that forms under these particular conditions. The significance of the $UMoO_6$ phase (Fig. 1 and Table 1) will be discussed in more detail in the discussion provided in Section 3.

2. Comparison of the model to experiment

As a benchmark of the thermodynamic treatment, predictions of the model were compared to measured data for fuel oxidation experiments conducted at the Atomic Energy of Canada Limited–Chalk River Laboratories (AECL–CRL). These experiments were

Table 1
Phase predictions for a four-additive SIMFUEL sample.

Predicted phase	Phase proportion (normalized to $UO_{2\pm x}$)
$UO_{2\pm x}$ solid phase with dilute fission products	1.00
Face centred-cubic noble metal solid phase	1.80×10^{-3}
Hexagonal close-packed noble metal solid phase	8.43×10^{-4}
Strontium–barium uranate solid phase ($(Sr/Ba)UO_4$)	3.29×10^{-5}
Cs_2MoO_4	1.11×10^{-7}
$UMoO_6$	2.48×10^{-3}

specifically used to test the capability of the model to predict the amount of oxygen acquired by the sample. In these experiments, a coulometric titration (CT) apparatus was used with UO_2 and SIMFUEL fuel samples under varying fuel oxygen potentials and temperatures. The CT apparatus is well suited for this examination because it is capable of creating and controlling precisely very low oxygen partial pressures (p_{O_2}) in the order of 10^{-10} atm to 10^{-19} atm at high temperature. A comparison of the model predictions with CT results is used to provide some corroboration of the integrated fuel/fission product model.

A review of the theory for coulometric titration operation is provided in Section 2.1. A comparison of the experimental results with the model predictions is given in Section 2.2.

2.1. Description and operation of the coulometric titration apparatus

The CT apparatus in Fig. 2 is comprised of two GSM5-EL cells manufactured by ZIROX Sensoren & Elektronik GmbH based in Germany, upstream and downstream of a sample furnace. This apparatus utilizes a given H_2 to H_2O ratio as the fundamental process to create low, stable oxygen partial pressures at a given temperature. The stability of the oxygen partial pressure at a fixed temperature is attained by the equilibrium ratio of partial pressures of hydrogen gas (p_{H_2}) and water vapour (p_{H_2O}) (i.e., H_2:H_2O). From the equilibrium state:

$$2H_{2(g)} + O_{2(g)} \leftrightarrow 2H_2O_{(g)} \tag{1}$$

the oxygen partial pressure (p_{O_2}) is obtained as follows:

$$p_{O_2} = \left(\frac{p_{H_2}}{p_{H_2O}}\right)^{-2} \cdot e^{\frac{\Delta G^o}{RT}} \tag{2}$$

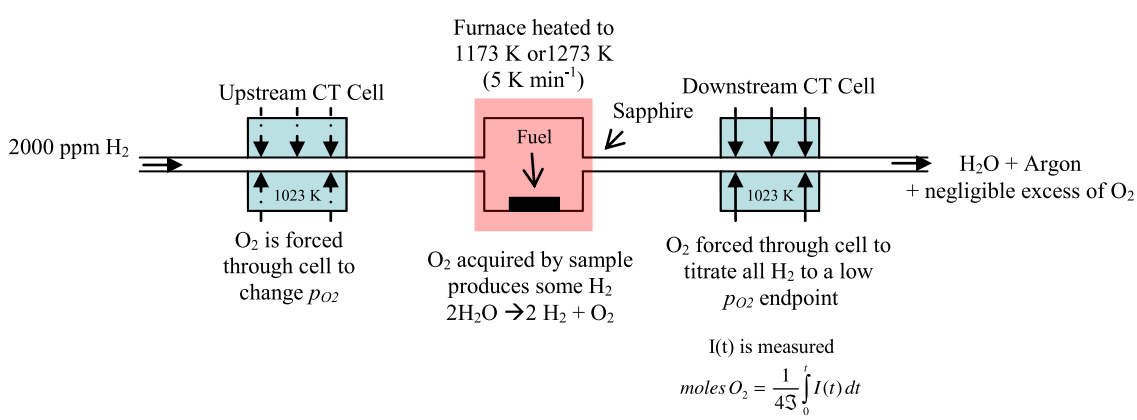

Fig. 2. Schematic diagram of coulometric titration apparatus [11,17].

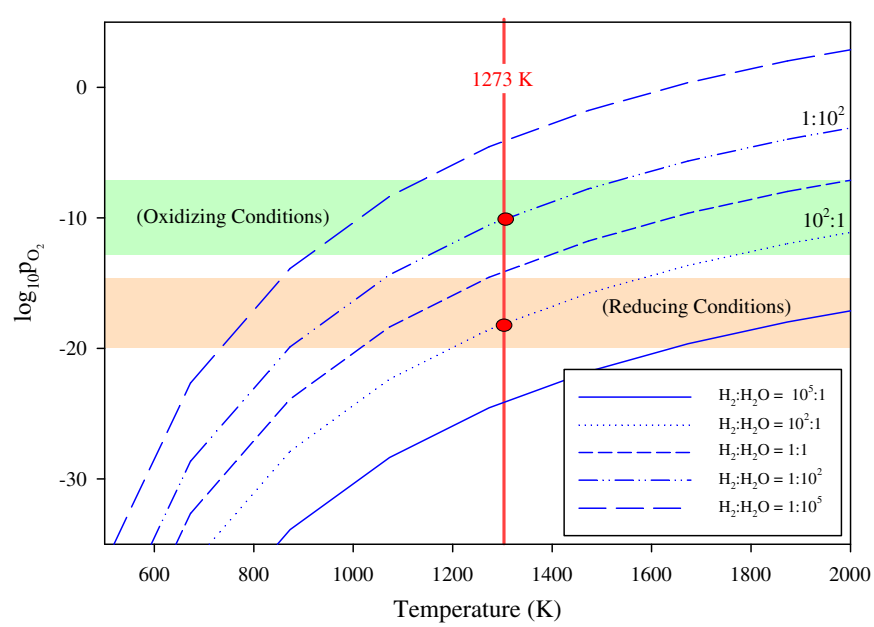

Fig. 3. Relationship between p_{O_2} and H_2:H_2O over a range of temperatures. Experimental oxidation and reducing conditions are marked by the green (upper) and orange (lower) bands, respectively. (For interpretation of the references to colour in this figure legend, the reader is referred to the web version of this article.)

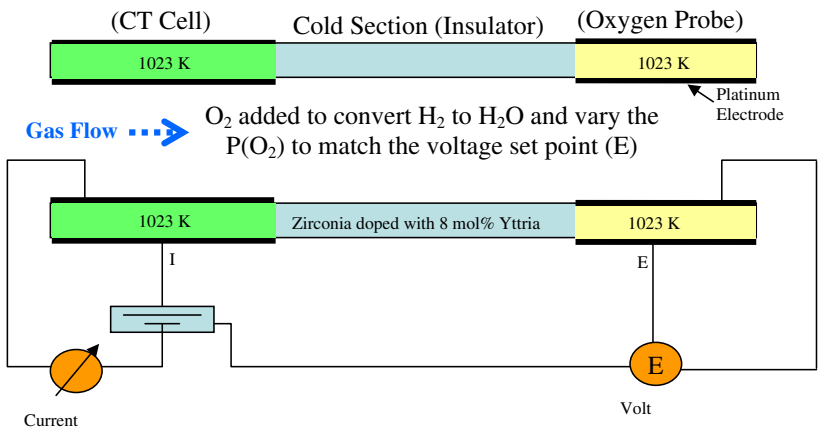

Fig. 4. Schematic diagram of coulometric titration (CT) cell [11].

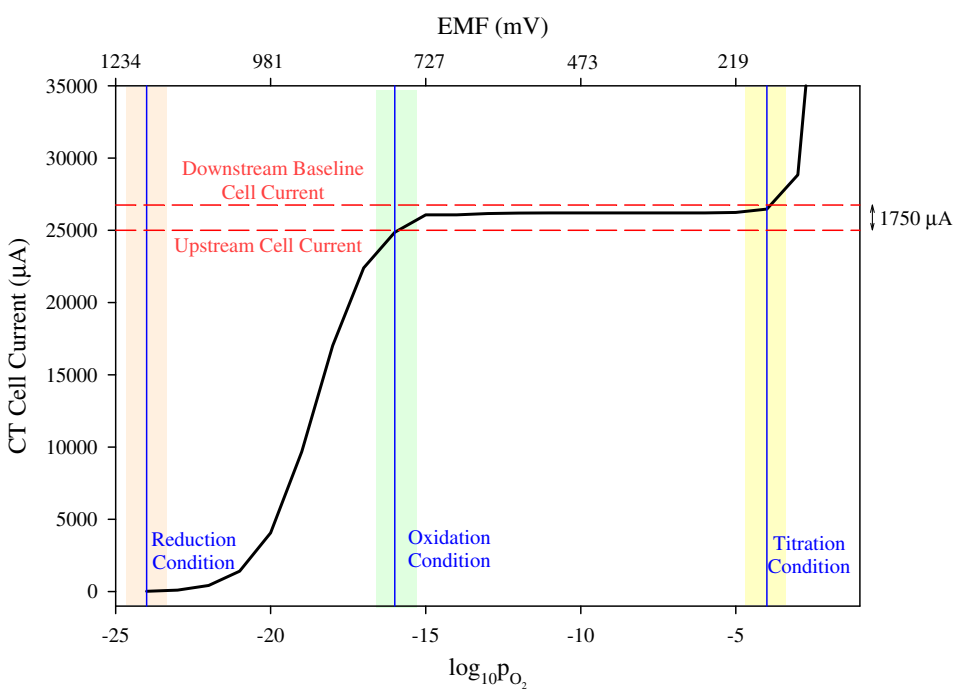

Fig. 5. Relationship between electromotive force (EMF), CT cell current and the partial pressure of O_2 at 1023 K for a 100 mL min^{-1} gas flow rate of a 1995 ppm H_2, 2 ppm H_2O and 0.9 ppm O_2 in argon gas mixture.

where ΔG^o is the standard Gibbs energy of reaction defined by Eq. (1) at temperature T and R is the gas constant.

As illustrated in Fig. 3, at 1273 K, the oxygen partial pressures required to oxidize and reduce a sample are attained with H_2:H_2O ratios of 1:10^2 and 10^2:1, respectively. The CT cell controls the H_2:H_2O ratio by regulating the electrolytic introduction of oxygen, some of which combines with the H_2 gas to produce H_2O vapour.

At the cell operational temperature (1023 K), which was fixed by the manufacturer, the solid electrolyte transports current by the movement of O^{2-} ions. The half cell reactions are:

$$\begin{aligned} &O_2 + 4e^- \rightarrow 2O^{2-}(\text{outside cell, high } O_2 \text{ concentration}) \\ &2O^{2-} \rightarrow O_2 + 4e^-(\text{inside cell, low } O_2 \text{ concentration}) \end{aligned} \tag{3}$$

The charge passed through the cell is proportional to the number of moles of oxygen transferred. Two moles of O^{2-} ions (or 1 mol O_2) correspond to four Faradays of charge (2 mol of O^{2-} ions = 4$\Im$).

The CT cell electrolyte material is used also as an oxygen sensor in an adjacent section of the electrolyte tubing where the open cell voltage (E) is related to the oxygen partial pressure (p_{O_2}) by the Nernst equation:

$$E = \frac{RT}{4\Im} \ln\left(\frac{p_{O_2\ \text{Atmospheric}}}{p_{O_2\ \text{Inside CT Tube}}}\right) \tag{4}$$

where $\Im$ the Faraday's constant. The two sections are mutually exclusive as they are separated by a cold zone (illustrated as a blue bar in Fig. 4). The separation is facilitated by the dependence of O^{2-} ion conductance to temperature. At low temperatures, the current of O^{2-} is impeded to the point where the ceramic becomes a virtual insulator [19]. For the ZIROX GSM5-EL cell, it was determined by the manufacturer[2] that a cell temperature of 1023 K was optimum. Temperatures well below the operational temperature have

[2] ZIROX Sensoren & Elektronik GmbH based in Germany.

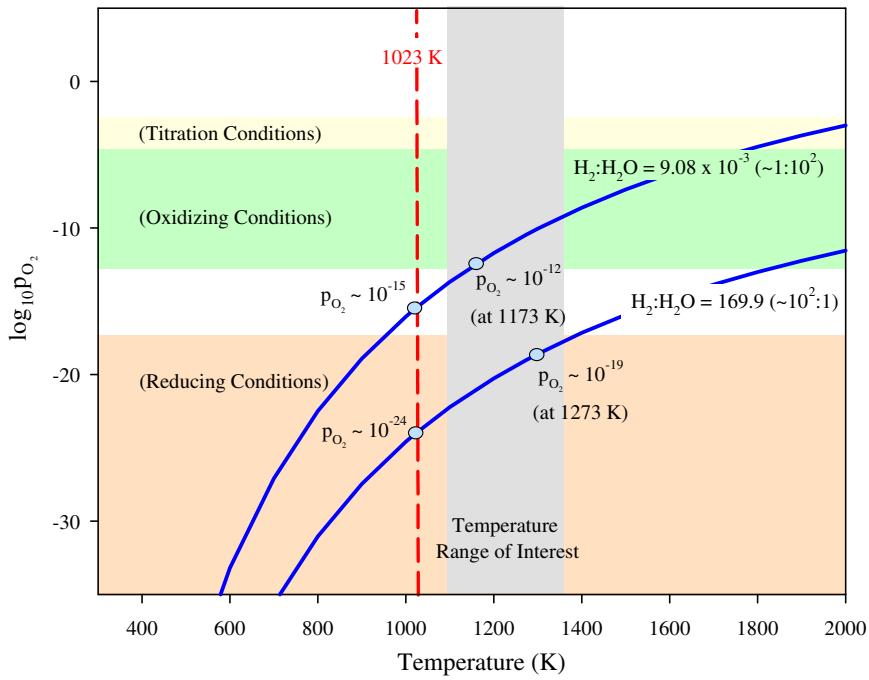

Fig. 6. The change in p_{O_2} as a function of temperature for a fixed H_2 to H_2O ratio for CT experimental settings.

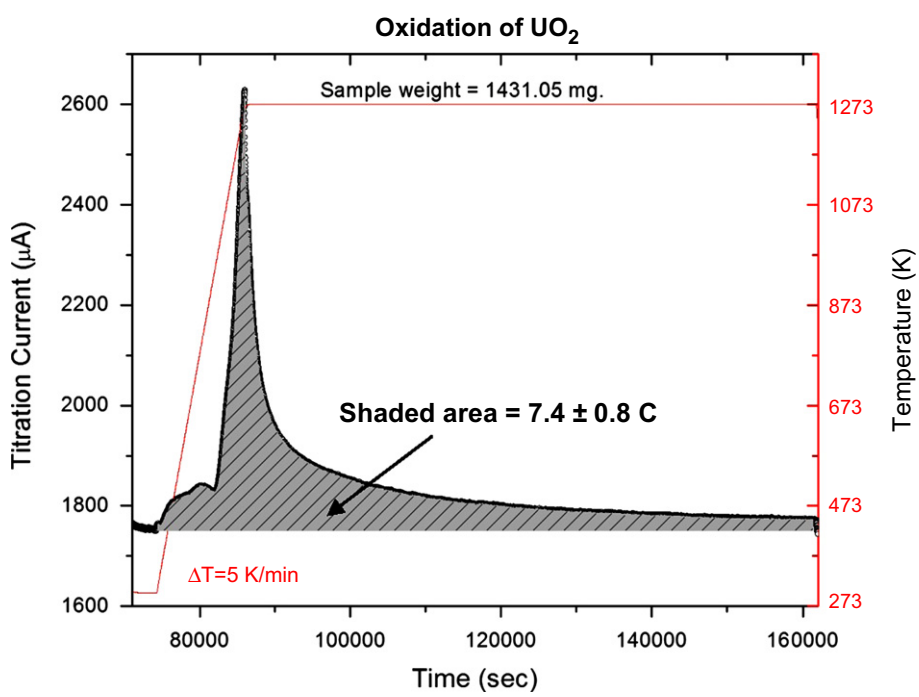

Fig. 7. CT oxidation results for a 1431.05 ± 0.05 mg of UO_2.

insufficient conductance of oxygen ions; at temperatures well above the operational temperature, semi-conduction is possible but the material is not longer a true electrolyte.

The ZIROX GSM5-EL cell utilizes a voltage feedback loop to control the oxygen partial pressure at the downstream oxygen sensor. The downstream sensor is set to a predetermined value and O^{2-} current is forced through the upstream section of the cell. The oxygen reacts with virtually all of the hydrogen in the gas mixture to create water vapour and a negligible surplus of oxygen; the passage of current through the cell will continue until the gas reaches a predetermined set point of oxygen partial pressure. The term "titration" only refers to the operation of the downstream cell.

In the complete CT apparatus (Fig. 2) two solid state cells are used, one upstream and one downstream of a sample furnace. Fuel samples are heated in the central furnace. The upstream cell controls the oxygen partial pressure of an argon–hydrogen gas mixture passing over the sample. The downstream cell passes a

current sufficient to convert the remaining H_2 to H_2O. The open circuit section of the downstream cell is set to a voltage associated with virtually complete conversion of the H_2 to H_2O, hence the term 'titration' in reference to the CT apparatus. The deviation in current from a defined baseline determined with no sample present provides the basis for measuring the oxygen pickup when a sample of UO_2 or SIMFUEL is analyzed in the apparatus. The relationship between open circuit voltages (E in Eq. (4)), O^{2-} currents, and oxygen partial pressures (p_{O_2}) for the two cells is illustrated in Fig. 5.

2.1.1. Reduction mode of operation

When the CT apparatus operates in a reduction mode, no current is passed through the upstream cell so that the oxygen partial pressure over the sample is dependent only on the feed gas composition. For a gas mixture of approximately 2000 ppm H_2 in argon, with a typical trace concentration of H_2O, the oxygen partial pressure is approximately 10^{-24} atm (at 1023 K) in the upstream cell (Fig. 5). The downstream cell passes a current of approximately 26,750 μA to titrate the hydrogen in the gas to water vapour to a very slight excess in oxygen partial pressure (10^{-4} atm at 1023 K) in the exiting gas (Fig. 5).

Table 2
Composition of SIMFUEL samples (in ppm) [20].

	Four-additives		11-Additives	
	ppm	±	ppm	±
Ba	9	2	1000	100
Ce	7	1	2700	300
Cs	0.11	0.03	–	–
La	3.5	0.7	900	200
Mo	900	100	180	40
Nd	18	4	4500	500
Pd	700	50	260	50
Rh	50	20	50	10
Ru	280	30	13	6
Sr	5	1	1600	200
U	890,000	40,000	880,000	40,000
Zr	7	1	2200	200

2.1.2. Oxidation mode of operation

When the CT apparatus is in an oxidationmode of operation, a current of approximately 25,000 μA is passed through the upstream cell to create a mixture with an H_2:H_2O ratio of $1{:}9.1 \times 10^{-3}$. This corresponds to an oxygen partial pressure of approximately 10^{-15} atm at 1023 K (Fig. 5). As the gas flow is oxidized partially by the upstream cell, the downstream cell only needs to pass a small current (~1750 μA) to titrate the remaining hydrogen in the gas to create an oxygen partial pressure of approximately 10^{-4} atm at 1023 K (Fig. 5). Any deviation from the baseline current indicates the amount of oxygen either acquired (if the downstream current is greater than baseline) or released by the sample (if the downstream current is less than baseline).

For a given flow of argon–H_2 gas with a known composition entering the apparatus, the same current is passed through the cells for both reduction and oxidation modes. In reduction mode, the downstream CT cell passes all the current (26,750 μA), but in the oxidation mode the current is distributed between the two CT cells.

The oxygen partial pressure created in the upstream cell at 1023 K is not the oxygen partial pressure over the sample at higher temperatures. Recall that the H_2:H_2O ratios for reducing and oxidizing conditions have been fixed at approximately 10^2:1 and 1:10^2, respectively. At reducing conditions, the oxygen partial pressure in the upstream cell is approximately 10^{-24} atm at 1023 K and 10^{-19} atm at 1273 K (in the furnace). At oxidizing conditions, the oxygen partial pressure is approximately 10^{-15} atm at 1023 K and approximately 10^{-12} atm at 1173 K. This increase in oxygen partial pressure is a result of the change in equilibrium constant (K_{eq}) for the dissolution of water ($H_2O \leftrightarrow H_2 + 0.5O_2$) as a function of temperature. The change in oxygen partial pressure as a function of temperature for the CT apparatus is shown in Fig. 6. H_2:H_2O ratios are fixed for both reduction ($1{:}1.7 \times 10^2$) and oxidation ($1{:}9.1 \times 10^{-3}$) conditions, and the oxygen partial pressure varies as a function of temperature.

In order to have confidence in the results from the CT apparatus, several components and set points were checked for proper operation. This included verifying the oxygen sensor in the downstream

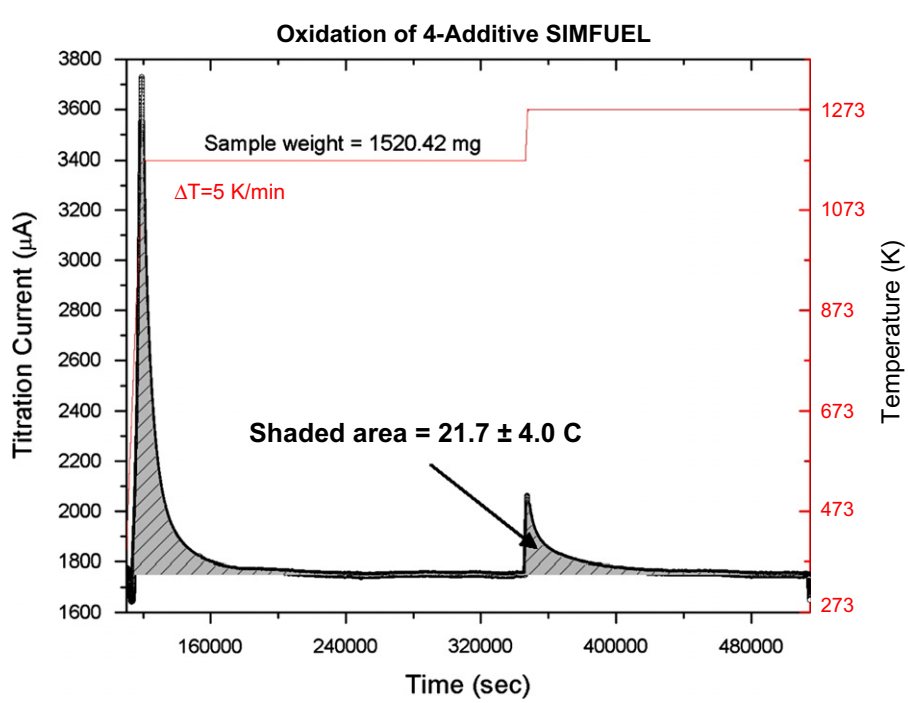

Fig. 8. Summary of results for oxidation of four-additive SIMFUEL at 1173 K and then 1273 K.

Table 3
Summary of CT results for UO_2 and SIMFUEL samples.

Sample type	Temperature (K)	Measured charge (C)
UO_2	1273	7.4 ± 0.8
SIMFUEL – four-additive	1173	16.9 ± 2.3
SIMFUEL – four-additive	1273	21.7 ± 4.0
SIMFUEL – 11-additive	1173	15.4 ± 3.1
SIMFUEL – 11-additive	1273	17.6 ± 5.9

Table 4
Comparison of updated irradiated CANDU fuel model to CT results for SIMFUEL samples.

Run	SIMFUEL sample	Temperature (K)	Measured charge (C)	Predicted charge (C)
Standard	UO_2	1273	7.4 ± 0.8	7.3 ± 0.3
1	Four-additive	1173	16.9 ± 2.3	16.1 ± 1.5
2	Four-additive	1273	21.7 ± 4.0	20.0 ± 1.6
3	11-additive	1173	15.4 ± 3.1	12.6 ± 1.4
4	11-additive	1273	17.6 ± 5.9	13.0 ± 1.4

CT cell, checking the flow meters, the overall leak tightness of the apparatus, and determining the baseline current condition in the downstream cell (1.750 ± 0.01 mA).

Each experimental run involved two steps. First, the sample was reduced at 1273 K to bring the sample to a known baseline state. Then, the sample was oxidized at 1173 K or 1273 K to obtain the amount of oxygen acquired by the sample. The oxidization and reduction furnace temperatures were selected (above that of the CT cell operational temperature of 1023 K) to increase the rate of oxygen acquisition or loss, so that the length of each experimental run could be completed in a reasonable amount of time.

2.2. Experimental results and model comparison

The results of the CT experiment with UO_2 and SIMFUEL samples are summarized in this section. The UO_2 case is included as a standard run to demonstrate the validity of the U–O model (i.e., for fresh fuel). This case is followed by the results of the SIMFUEL analysis.

2.2.1. UO_2 fuel sample

The oxidation behaviour of UO_2 is well known at temperatures below 1673 K and provides a standard case for comparison with the irradiated CANDU fuel model predictions. To ensure that the CT apparatus was operating as expected, 1431.05 ± 0.05 mg or $0.52996 \pm 0.00002 \times 10^{-2}$ mol of pure UO_2 was oxidized at 1273 K.

The measured CT result for UO_2 was 7.4 ± 0.8 C, which represents an O_2 pickup of $1.9 \pm 0.2 \times 10^{-5}$ mol. The shape of the titration current curve (Fig. 7) measured in the downstream cell indicates that the UO_2 sample acquired oxygen.

2.2.2. SIMFUEL samples

The SIMFUEL samples provide a composition of fission products in nuclear fuel without the associated radioactive risk. This facilitates material handling in the CT experiments. In addition, the SIMFUEL samples are convenient for benchmarking as the material composition for a given simulated fuel burnup is well-established [18,20].

Two SIMFUEL samples were investigated; one with four-additives and another with 11-additives. The four-additive SIMFUEL contained mainly noble metals (Mo, Pd, Rh and Ru). The 11-additive sample was a mixture of noble metals, Zr, Ba, Sr and the rare earth elements (La, Ce, and Nd). All SIMFUEL samples were manufactured at Atomic Energy of Canada Limited–Chalk River Laboratories [18]. The compositions of each are listed in Table 2.

A typical result for the four-additive SIMFUEL is illustrated in Fig. 8. The measured number of Coulombs of charge (proportional to the number of moles of oxygen passing through the cell) for each experiment is summarized in Table 3.

The amount of oxygen acquired (in terms of charge) as predicted by the model can be compared to the measurements as shown in Table 4. Agreement is generally seen within the experimental error and model uncertainty.

The uncertainty for each predicted value was found with a sensitivity analysis, where the temperature, oxygen partial pressure (p_{O_2}) and compound composition (amount of each element) were varied within their individual uncertainties. The largest calculated uncertainty is indicated in Table 4.

The thermochemical model was assembled from many sources of data and treatments. However, the selected fuel oxidation

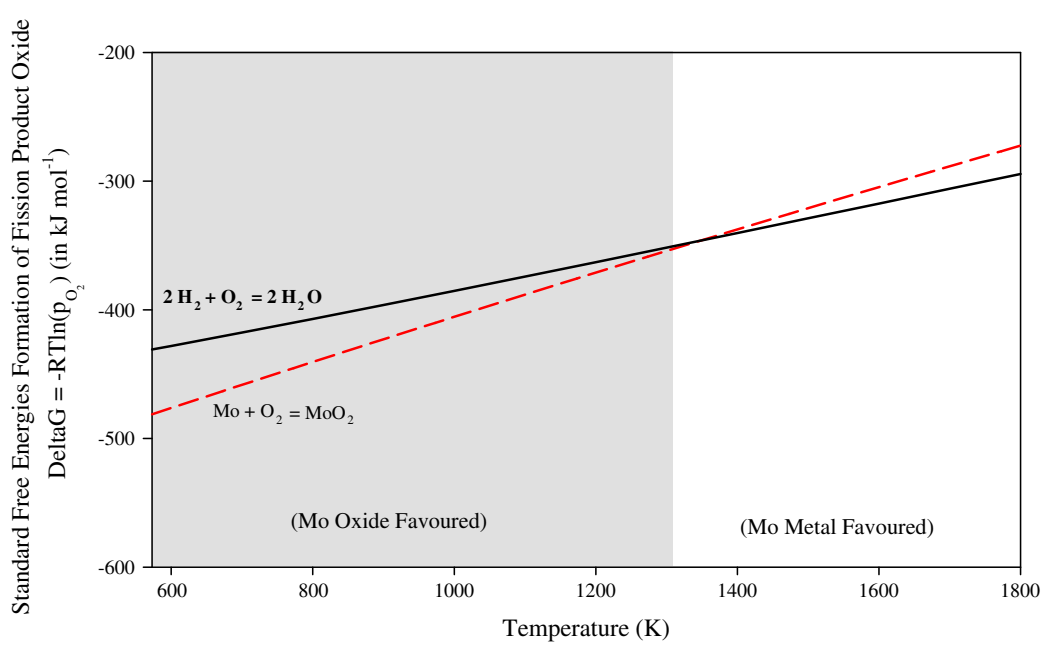

Fig. 9. Ellingham diagram comparing H_2O and MoO_2. The position of the H_2O/H_2 (solid black) line applies to a ratio of 1:1; the line shifts upward when the H_2O/H_2 ratio is increased.

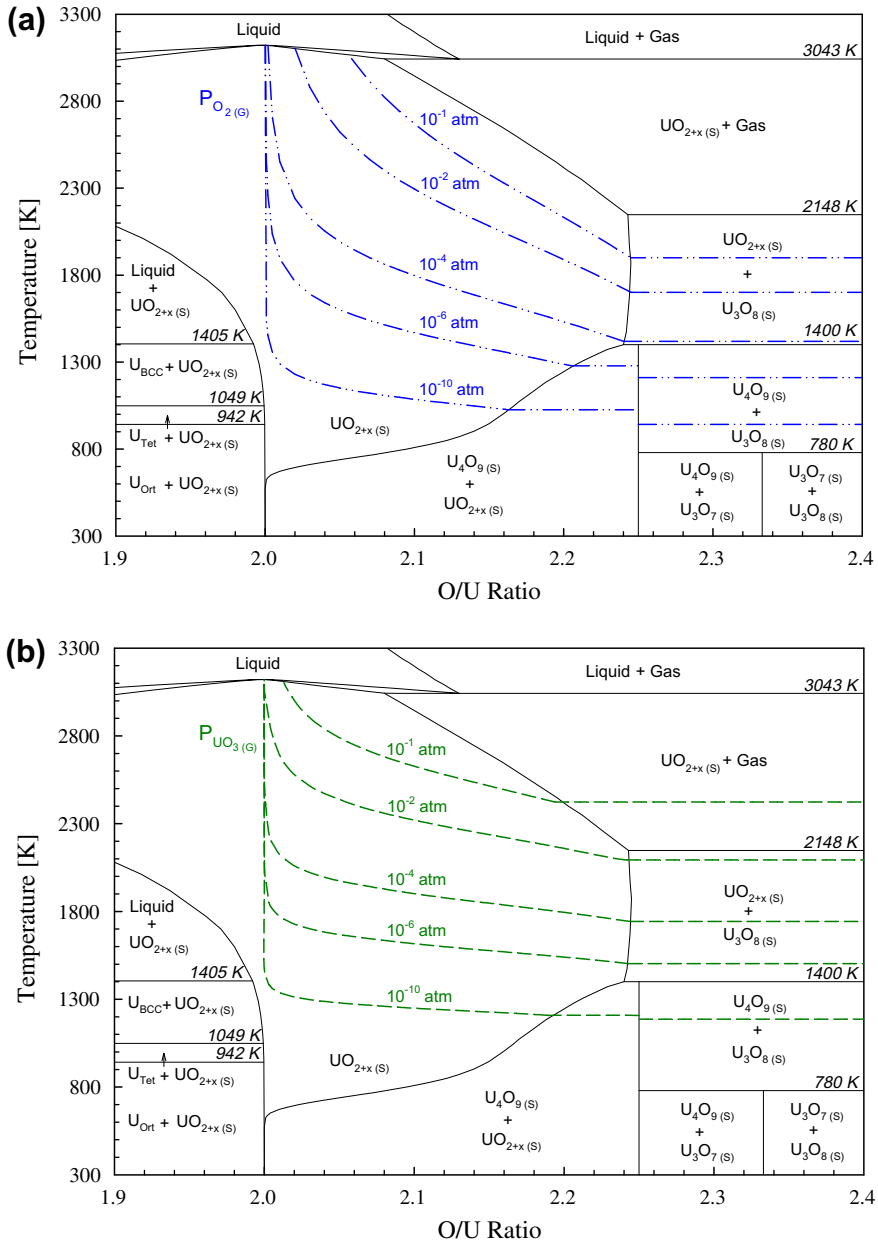

Fig. 10. Calculated U–O binary phase diagram with isobaric lines of (a) O_2 and (b) UO_3 partial pressure.

experiments at Atomic Energy of Canada Limited–Chalk River Laboratories suggest that the integrated fuel model is reasonable. Nevertheless, a further investigation of the 11-additive SIMFUEL sample was undertaken to discover if any other compounds might contribute to oxidation. The 11-additive SIMFUEL material is rich in Ba, Sr, Zr and the rare earths (Nd, Ce and La). A review of the Ba and Sr compounds indicated that the model representation was faithful to published values. A further investigation for the zirconate and rare earth components also confirmed that the current treatment conforms to the literature.

3. Discussion

3.1. The importance of molybdenum with respect to fuel oxidation

The relationship between oxygen partial pressure and oxidation (x) of pure UO_{2+x} is well known, however it is disturbed by the presence of fission product elements, which can have vastly different abilities to combine with oxygen. Since it is the oxygen combined in water that is the source of oxygen for in-reactor defective fuel oxidation, it is the relative stability of H_2O to that of an oxide that is especially significant. This relationship is shown in the Ellingham diagram (Fig. 9) that depicts the Gibbs energy of formation of H_2O and MoO_2. Expressing the Gibbs energy of formation for both compounds on a mole of O_2 basis facilitates comparison.

Other oxides not shown in Fig. 9, such as PdO, lie far above the H_2O line and therefore do not easily oxidize but tend to exist in oxidized fuel as metal; UO_2 and the rare earth oxides on the other hand lie very far below the H_2O line and are very stable as oxides when in contact with H_2O. Oxidation measurements, under carefully controlled conditions, therefore provide a particularly good test for the nuclear fuel model outlined above and put a strong focus on molybdenum. The experimental approach used in this work is clearly only one of many that could be used to identify potential improvements or contribute to the validation of the thermody-

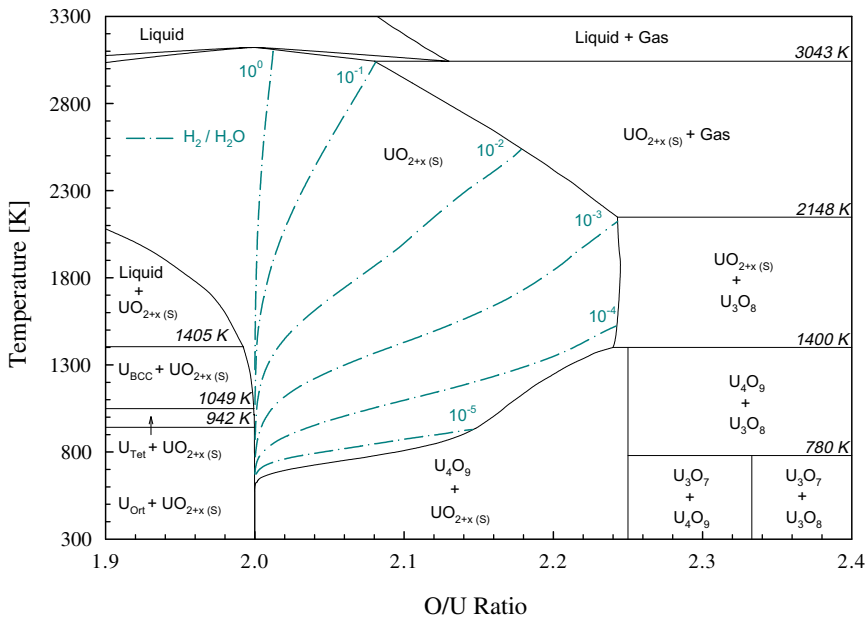

Fig. 11. Calculated U–O binary phase diagram with lines of constant H_2/H_2O.

namic fuel treatment. However, this experiment is of direct value to the testing of the fuel thermochemical model in relation to its use in fuel oxidation computations pertinent to a sheathing breach.

The concentration of molybdenum in the SIMFUEL samples and ability of molybdenum to exist as a metal (Mo) or oxide (MoO_2), as illustrated in Fig. 9, was a significant clue in directing the revision of the model in Ref. [13] by the addition of $UMoO_6$ [21,22] compound and a small reduction of the solubility of MoO_2 in the $UO_{2\pm x}$ solid solution. These modifications were necessary to bring the model predictions and measured results (Table 4) into agreement because of the buffering nature of Mo and its effect on oxygen potential (*e.g.*, the number of moles of oxygen absorbed by the fuel sample at a given oxygen partial pressure).

3.2. Model application

The current treatment has several direct applications. These include:

(i) *Predicting the gaseous proportion of partial pressure over the fuel as a function of temperature.* The current thermodynamic treatment provides a means to add isobaric lines of O_2 and UO_3 partial pressure to the phase diagram as shown in Fig. 10. Since the partial oxygen pressure in the UO_{2+x} field is very low, it is useful to express this partial pressure as the equivalent H_2/H_2O (Fig. 11) proportion using the temperature dependent equilibrium constant for the process:

$$H_2O \Longleftrightarrow H_2 + \frac{1}{2}O_2 \tag{5}$$

The current treatment is in excellent agreement with the thermodynamic treatments of Lindemer–Besmann [23] and Blackburn [24]. Similarly, the (H_2/H_2O) variation of the UO_{2+x} non-stoichiometry can be derived as shown in Fig. 11. Little difference is seen for the prediction of the atmospheric oxygen potential between light and heavy water. It is noteworthy that the constant ratio lines converge about the 2:1 ratio for the O:U proportion at temperatures below about 773 K. This implies that with defective fuel contact of steam with UO_2 below 773 K imparts very little disturbance to the UO_2 stoichiometry, i.e., higher temperatures are required to create a significantly hyperstoichiometric UO_2.

(ii) *Predicting phase stability and proportion of fuel as a function of burnup, oxygen potential and temperature.* The model can be used to determine the element and compound inventory of intact fuel. However, this computation is complicated by a continually changing fission product concentration, diffusion, and oxygen potential with irradiation and decay, as well as by very steep temperature gradients within the fuel.

Also, knowledge of the gaseous fission product inventory is useful to determine the potential health hazards to plant personnel and the composition of corrosive fission products that may lead to stress corrosion cracking (e.g., quantities of I and Cs). Fuel designers would benefit from this knowledge, especially where the quantities of fission products are expected to be much higher than in current fuel designs.

3.3. Model limitations and future work

The thermochemical computations implicitly assume that the system is in (local) thermodynamic equilibrium. However, during and after irradiation, the chemistry of the fuel-fission product system is complicated by several phenomena where: (i) the fission product concentrations increase gradually with irradiation; (ii) the chemical properties of the fission products change after irradiation because of radioactive β-decay; (iii) the oxygen chemical potential of the fuel changes with fuel burnup and the related production of fission products which can alter the oxygen-to-metal ratio of the fuel; and (iv) the axial and radial temperature gradients affect the distribution of the elements into phases and lead to compositional gradients with material transport by thermal diffusion processes [2,5,25,26]. There can be substantial migration of some elements, particularly the volatile fission products, which can contribute to a gradient in the oxygen chemical potential in the pellet. Equilibrium calculations can only be used as a basis for estimation of the chemical state. To accurately model element migration the equilibrium calculations must be paired with a material transport analysis, this requires numerical data for the heat of transport of all elements (some of this transport data are not well known) [27].

As such, the thermochemical model must be incorporated into a fuel performance/fission product release code in order to mechanistically couple the fission product chemistry with the fission product transport within the fuel matrix and fuel-to-clad gap [28]. With this incorporation, the model can be further used to assess the gaseous and aqueous phases that may be released during a fuel cladding breach. Moreover, in the case of failed-fuel pins, the ingress of water for water-cooled reactors into the element can result in further reactions with the fuel and fission products [29,30]. The cladding can participate in reactions with the fission products delaying their release into the fuel-to-clad gap or into the coolant system with the possibility of fuel-rod failure [31]. Moreover, the corrosive behaviour of the fission products in the fuel-to-clad gap can affect fuel performance, possibly leading to fuel failure as a consequence of environmentally-assisted stress corrosion cracking during power ramping manoeuvres [32–34]. The fission products, fuel and cladding can also interact among themselves, as well as with surrounding structural materials, during high temperature reactor accident conditions leading to the possibility of fuel dissolution and material relocation [10,35–40]. Such detailed analysis would therefore require further model development with the implementation of the given and extended thermochemical model into other fuel performance and safety codes.

4. Conclusions

1. A comprehensive thermochemical treatment for irradiated fuel has been assembled to determine the chemical state of elements associated with the appearance of new and changing phases with fuel burnup. The thermodynamic functions can be used in a Gibbs energy minimizer to predict the chemical state of the fuel and fission product constituents produced as a result of the fissioning of the fuel.
2. The model predictions are within the uncertainty of critical benchmarking coulometric titration experiments on UO_2 and SIMFUEL samples.
3. The model can be used to assess the chemical state of the fuel and fission products, including the chemical potential of intact and defective fuel with burnup. The thermodynamic database with a stand-alone Gibbs energy minimizer routine could be implemented into a fuel performance/fission product release code in order to link the fuel chemistry with fission product transport phenomena.

Acknowledgments

The authors would like to acknowledge the Natural Science and Engineering Research Council, CANDU Owners Group, the University Network of Excellence in Nuclear Engineering and the Department of National Defence for support of this work. The authors would like to acknowledge the assistance of M. Piro with this paper. Finally, the authors wish to thank L. Dickson, R. Verrall, and H. Hamilton of Atomic Energy of Canada Limited for their interest and support, which has made this on-going collaboration possible.

References

[1] W.H. Hocking, A.M. Duclos, L.H. Johnson, J. Nucl. Mater. 209 (1994) 1–26.
[2] H. Kleykamp, J. Nucl. Mater. 131 (1985) 221–246.
[3] E.H.P. Cordfunke, R.J.M. Konings, J. Nucl. Mater. 152 (1988) 301–309.
[4] H. Kleykamp, J. Nucl. Mater. 171 (1990) 181–188.
[5] H. Kleykamp, Nucl. Technol. 80 (1988) 412–422.
[6] D.N. Sah, C.S. Viswanadham, S. Kumar, P.R. Roy, Nucl. Technol. 85 (1989) 136.
[7] I. Johnson, C.E. Johnson, J. Nucl. Mater. 154 (1988) 67–73.
[8] D. Cubicciotti, J.E. Sanecki, J. Nucl. Mater. 78 (1978) 96.
[9] Hj. Matzke, Radiat. Eff. 53 (1980) 219–242.
[10] J.H. Gittus, J.R. Mathews, P.E. Potter, J. Nucl. Mater. 166 (1989) 132–159.
[11] W.T. Thompson, B.J. Lewis, E.C. Corcoran, M.K. Kaye, S.J. White, F. Akbari, Z. He, R. Verrall, J.D. Higgs, D.M. Thompson, T.M. Besmann, S.C. Vogel, Int. J. Mater. Res. 98 (2007) 10 1004–1011.
[12] M.H. Kaye, B.J. Lewis, W.T. Thompson, J. Nucl. Mater. 366 (2007) 8–27.
[13] E.C. Corcoran, Doctoral Thesis, Royal Military College of Canada, Kingston, Ontario, 2009.
[14] B.J. Lewis, W.T. Thompson, F.C. Iglesias, R. Koning (Ed.), Comprehensive Nuclear Materials, Elsevier, in press (Chapter 42).
[15] A.D. Pelton, W.T. Thompson, Prog. Solid State Chem. 10 (Part 3) (1975) 119–155.
[16] M.H. Piro, M.J. Welland, B.J. Lewis, W.T. Thompson, D.R. Olander, in: Proc. of 2009 Water Reactor Fuel Performance Meeting (Top Fuel), Paris, France, 2009.
[17] R.A. Verrall, Z. He, J. Mouris, J. Nucl. Mater. 344 (1–3) (2005) 240–245.
[18] P.G. Lucuta, R.A. Verrall, H.j. Matzke, B.J. Palmera, J. Nucl. Mater. 178 1 (1991) 48–60.
[19] D.J. Parks, K.L. Scholl, E.A. Fletcher, Energy (1988) 121–136.
[20] J. Mouris, E.C. Corcoran, Private Communication, AECL–CRL, March 2007.
[21] S. Dash, K. Jayanthi, Z. Singh, N.D. Dahale, S.C. Parida, V.S. Iyer, J. Alloys Compd. 296 (2000) 166–169.
[22] S.R. Dharwadkar, J. Mater. Sci. Lett. 5 (1986) 1003–1006.
[23] T.B. Lindemer, T.M. Besmann, J. Nucl. Mater. 130 (1985) 473–488.
[24] P.E. Blackburn, J. Nucl. Mater. 46 (1973) 244–252.
[25] S. Imoto, J. Nucl. Mater. 140 (1986) 19–27.
[26] H. Kleykamp, J. Nucl. Mater. 84 (1979) 109–117.
[27] H. Kleykamp, J. Nucl. Mater. 344 (2005) 1–7.
[28] M.S. Veshchunov, R. Dubourg, V.D. Ozrin, V.E. Shestak, V.I. Tarasov, J. Nucl. Mater. 362 (2007) 327–335.
[29] J.D. Higgs, B.J. Lewis, W.T. Thompson, Z. He, J. Nucl. Mater. 366 (2007) 99–128.
[30] H. Kleykamp, J. Nucl. Mater. 248 (1997) 209–213.
[31] T. Arima, T. Masuzumi, H. Furuya, K. Idemitsu, Y. Inagaki, J. Nucl. Mater. 301 (2002) 90–97.
[32] P.S. Sidky, J. Nucl. Mater. 256 (1998) 1–17.
[33] P. Jacques, F. Lefebvre, C. Lemaignan, J. Nucl. Mater. 264 (1999) 239–248.
[34] P. Jacques, F. Lefebvre, C. Lemaignan, J. Nucl. Mater. 264 (1999) 249–256.
[35] A.W. Cronenberg, D.J. Osetek, J. Nucl. Mater. 149 (1987) 252–260.
[36] R. de Boer, E.H.P. Cordfunke, J. Nucl. Mater. 240 (1997) 124–130.
[37] B.J. Lewis, B.J. Corse, W.T. Thompson, M.H. Kaye, F.C. Iglesias, P. Elder, R. Dickson, Z. Liu, J. Nucl. Mater. 252 (1998) 235–256.
[38] S. Sunder, Nucl. Technol. 144 (2003) 259.
[39] B.J. Lewis, R. Dickson, F.C. Iglesias, G. Ducros, T. Kudo, J. Nucl. Mater. 380 (2008) 126–143.
[40] B.J. Lewis, F.C. Iglesias, R.S. Dickson, A. Williams, J. Nucl. Mater. 394 (2009) 67–86.